International Journal for Uncertainty Quantification, 4 (3): 185–204 (2014)

UNCERTAINTY QUANTIFICATION IN DYNAMIC SIMULATIONS OF LARGE-SCALE POWER SYSTEM MODELS USING THE HIGH-ORDER PROBABILISTIC COLLOCATION METHOD ON SPARSE GRIDS

Guang Lin,[1,] Marcelo Elizondo,[1] Shuai Lu,[1] & Xiaoliang Wan[2]*

[1] *Pacific Northwest National Laboratory, 902 Battelle Boulevard, Richland, Washington 99352, USA*

[2] *Department of Mathematics, Louisiana State University, Baton Rouge, Louisiana 70803, USA*

Original Manuscript Submitted: 09/26/2012; Final Draft Received: 06/24/2013

This paper employs a probabilistic collocation method (PCM) to quantify the uncertainties in dynamic simulations of power systems. The approach was tested on a single machine infinite bus system and the over 15,000 -bus Western Electricity Coordinating Council (WECC) system in western North America. Compared to the classic Monte Carlo (MC) method, the PCM applies the Smolyak algorithm to reduce the number of simulations that have to be performed. Therefore, the computational cost can be greatly reduced using PCM. A comparison was made with the MC method on a single machine as well as the WECC system. The simulation results show that by using PCM only a small number of sparse grid points need to be sampled even when dealing with systems with a relatively large number of uncertain parameters.

KEY WORDS: *uncertainty quantification, Monte Carlo method, probabilistic collocation method, generalized polynomial chaos*

1. INTRODUCTION

Uncertainty quantification (UQ) can provide important information for power grid operations, such as the margin added on to simulation results to determine power transfer limits on transmission lines. A power system is inherently stochastic, with its generator and load parameters changing over time. Environmental and human factors also affect the parameters. The increasing penetration of variable renewable energy resources, such as wind and solar, further increases the level of uncertainty. It is becoming more and more imperative to acquire accurate knowledge of the uncertainties in dynamic simulations used to guide operations. UQ can provide a meaningful probabilistic measure and an error bar for many essential power grid applications (e.g., contingency analysis, automatic generation control, and optimal power flow) to improve the operational efficiency and reliability of a power system [1–3].

Because of the lack of knowledge on some parameters in dynamic power system modeling, such as the motor load percentage in the representation of system loads, and the wind speed and direction at wind farms, the values predicted by dynamic simulations will carry some levels of uncertainty. The main goal of UQ in this paper is to quantify the uncertainty in the power system with dynamic simulation results. The parameter uncertainties can be modeled as random variables with a probability density function (PDF). The output uncertainties will be represented using error bars and confidence levels. For example, an estimation of a 1000 MW power flow with ± 10 MW error bars (95% confidence interval) carries more information than a simple point estimation of 1000 MW. Meanwhile, an estimate of 1000 MW $\pm$ 10 MW is more accurate than an estimate of 1000 MW $\pm$ 500 MW. By adding error bars with a

*Correspond to Guang Lin, E-mail: kdalbey@sandia.gov

2152–5080/14/$35.00

confidence level, information that is more complete and accurate can be revealed to provide helpful guidance to grid operations.

Power system models can have many sources of uncertainty. Intermittent renewable generation provides a source of uncertainty [4, 5]. Generator models also have uncertainties, for example, discrepancies between the governor system responses of real systems and their models were detected in [6]. In [7] large discrepancies between real system behavior and the behavior obtained by dynamic models were shown. Load models, high voltage direct current (HVDC) transmission models, and generator models were the main sources of uncertainty. Consequently, several improvements in the model have been implemented, including regular testing and validation of individual components like generators. Currently there are ongoing efforts in load modeling and renewable generation modeling through modeling task forces [8]. However, UQ has not yet been implemented in power system analysis and simulation practice.

Two attempts have been made to include the effect of parameter uncertainties in the dynamic models of the power system. First, trajectory sensitivity was used to obtain a first-order approximation of the trajectory corresponding to a perturbed parameter set [9, 10]. This approach uses an augmented model of the system that is linearized to approximate the effect of uncertain parameters around a nominal system trajectory. The linearization of the trajectory sensitivity equations implies that results are valid for small perturbations around the trajectory. A Monte Carlo (MC) simulation can be applied to this trajectory sensitivity model to quantify uncertainties. The second attempt to perform UQ in the power system model was a probabilistic collocation method (PCM) [11]. This method allows the uncertainty in transient behavior of power systems to be studied by using a handful of simulations. The simulation results are used by PCM to build a polynomial chaos-based model that maps uncertain parameters to outcomes of interest. While PCM was used to quantify the uncertainty of a reduced order system (16 generators and 63 loads), it was recognized that the required number of simulations for PCM grows quickly for multiple uncertain parameters. In [11], only a sensitivity method was used to rank the most important uncertain parameters to reduce the number of simulations. In this paper, we use a full model of the western interconnection (3307 generators and 8230 loads) with 21 uncertain parameters. In addition, in a different technique from the PCM used in [11], our PCM uses sparse grids based on the Smolyak algorithm for a relatively large number of uncertainty parameters.

The methods for quantifying uncertainty levels depend on how the noises are modeled. In [12], linear models and Gaussian (normal) noises were assumed, and analytical approaches were used to quantify state prediction errors. Note that in this approach, the linearity and Gaussian noise assumptions reduce the computation intensity by providing analytical solutions. However, the assumptions limit the applicability of the method due to reduced accuracy from linear approximation and the limited noise model. In [13], a fuzzy linear state estimator (SE) model was used to quantify the uncertainty based on a fuzzy linear regression model. In [14, 15], a weighted least square (WLS) method was used to obtain point estimation and then a linear programming (LP) method was used to find the upper and lower bounds of the estimated states. The linear approximation was used in formulating the constraints. Also, one LP problem needed to be solved for quantifying the uncertainty of each individual estimated variable. With such a large number of estimated variables, this method requires extremely large computational power.

For a more general uncertainty distribution and a nonlinear model, there is no general analytical solution to quantify prediction uncertainty. To circumvent this difficulty, numerical approaches (e.g., MC methods) are usually used. The MC method calculates the prediction errors by repeatedly sampling the original parameter distribution. The MC method is widely used for studying statistical problems because of its simplicity. However, the number of samples required by the MC method is very large and increases with the dimensionality of the problem. The current *Western Electricity Coordinating Council* (WECC) power system has over 15,000 buses (i.e., over 30,000 states) and the number of MC samples is prohibitively large.

To overcome the computational problem brought in by the MC method, a probabilistic collocation method [16, 17] is applied in this paper to reduce the number of samples while maintaining the estimation accuracy. It is shown through simulations that the collocation method uses a smaller number of ensembles than the MC method to represent the uncertainty distribution.

The purpose of this paper is to develop a general method to quantify the uncertainty for dynamic power system modeling with a manageable computational burden. The paper is organized in the following way. In Section 2, the PCM is described and applied to quantify the uncertainty in dynamic power system modeling. In Section 3, simulation results from a single machine infinite bus system model and a WECC power system model are used to evaluate the

performance of the PCM and a comparison is made with the MC method. Section 4 draws the conclusion and provides some discussion about the potential application of the method and future works. The choices of collocation points are discussed in the Appendix.

2. UNCERTAINTY QUANTIFICATION ALGORITHMS

In modeling dynamic power systems, many parameters and measurements are subject to uncertainties. To estimate the uncertainty propagation, these uncertain variables are modeled as random variables with some known random distributions. MC simulations and other stochastic methods can be performed to estimate the output uncertainty. One disadvantage of the MC approach is its slow convergence rate. To speed up the convergence and reduce the computational cost, a PCM approach is introduced in this section. This approach can greatly reduce the number of ensemble runs for a moderate number of uncertain variables. The PCM approach was first introduced by Tatang and McRae [17] and has been recently extended by Xiu and Hesthaven [18]. Consider the stochastic equation

$$L(\mathbf{x}, t, \xi(\omega); u) = f(\mathbf{x}, t; \xi(\omega)) \tag{1}$$

where $u(\mathbf{x}, t; \xi)$ is the solution of Eq. (1), L is a general differential operator, $\mathbf{x} \in R^{d_s}$ (real vector with d_s number of entries), $d_s = 1, 2, 3$, is a physical space and t is time. In contrast to the Galerkin projection [19], in the collocation formulation, delta functions $\delta(\xi - \xi_k)$ are employed as test functions, $k = 0, ..., M-1$, where $\{\xi_k\}$ is a proper set of grid (quadrature) points on the support of $\xi(\omega)$ and M is the number of random dimensions. Applying the collocation projection on both sides of Eq. (1) results in $L(\mathbf{x}, t, \xi_k; u) = f(\mathbf{x}, t; \xi_k)$. The main advantage of the PCM over the Galerkin projection method of [19] is that the resulting set of deterministic equations is uncoupled for any form of the nonlinear operator L and these equations have the same form as the deterministic equations. The Galerkin projection formulation for the nonlinear operator L results in a system of coupled ordinary or partial differential equations. Hence, for complex nonlinear systems, such as power systems, the collocation projection method is easier to implement than the standard Galerkin projection method.

The general procedure for the PCM approach is

1. Generate N_c prescribed number of collocation points as independent random inputs based on cubature formula.
2. Solve the deterministic problem at each collocation point.
3. Evaluate the statistics of the random solution using the corresponding quadrature rule, e.g.,

$$< u(x,t) > = \int u(x,t;\xi) f(\xi) d\xi \approx \sum_{k=1}^{N_c} u(x,t;\xi_k) w_k, \quad \sigma(u)(x,t) = \sqrt{\sum_{k=1}^{N_c} u^2(x,t;\xi_k) w_k - < u >^2},$$

where $u(x, t; \xi)$ is the solution, $f(\xi)$ is the probability density function PDF of random variable ξ, N_c is the number of sparse grid points, and $\{w_k\}$ is the integration weight, which is the combination of the Gauss integration weight in each random dimension. In the second step of the PCM approach, any existing deterministic code can be used to solve power system equations. Here, Gauss cubature points are used as the collocation point set. Extensive reviews on the construction of cubature formula are covered in [20, 21]. The choice of collocation points is discussed in the Appendix.

3. UNCERTAINTY QUANTIFICATION FOR A SINGLE MACHINE INFINITE BUS MODEL AND WECC SYSTEM MODEL

Traditionally, uncertainty can be estimated using the MC method. The MC method estimates the uncertainty by repeatedly sampling the original random distribution. The MC method is widely used for studying statistical problems because of its simplicity and ease-of-use. However, the number of samples required by the MC method is very large

and increases with the complexity of the problem. Current western North American WECC power system models have over 15,000 buses (i.e., 30,000 states) and the required number of MC samples is prohibitively large.

To overcome this difficulty, a PCM approach is used to reduce the number of samples, while maintaining the estimation accuracy. The PCM approach uses a lesser number of samples than the MC method to represent the uncertainty distribution. Recently the PCM and polynomial chaos approach have been successfully employed to conduct uncertainty quantification for power systems [11, 22–25]. An alternative method is unscented transformation [26–28], which approximates a probability distribution using a small number of carefully chosen test points.

3.1 Formulation for a Single Machine Infinite Bus System

The equations in this paper have been modified from [29], Sections 3.6.5 and 13.3. The following equations consider the second-order generator model (classical model). This model does not take into account the field voltage dynamics; it considers instead the generator as a constant voltage behind a reactance.

Consider the following system. The system consists of a voltage source (with transient voltage E') connected to a terminal bus (with voltage E_t) through an internal impedance Z'_d; and the terminal bus is connected to an infinite bus (with voltage E_B) through a transmission line with impedance Z_E. The infinite bus is defined as a bus that can take as much power as provided by the generator without affecting its voltage.

As shown in Fig. 1, the rotor angle is $\delta = \theta - \theta_t$. E and E' denote voltage and transient voltage, I denotes current, R_a is the armature resistance per phase, X'_d denotes the generator transient reactance of a synchronous machine, θ denotes angle, and $\emptyset$ is the phase angle (angle difference between terminal voltage and current). X_E is the transmission line reactance. The letter j in complex impedance is called the j operator. The formulation for a systematic solution which is extendable to multimachine system modeling is listed as follows.

3.1.1 Equations of Motion

$$p\triangle\omega = \frac{1}{2H}\left(T_m - T_e - K_D\triangle\omega\right)$$

$$p\delta = \omega_0\triangle\omega$$

where $p = d/dt$ is the derivative operator, $\triangle\omega$ is the rotor speed deviation per unit, H is the inertia constant, T_m is the mechanical torque, T_e is the electrical torque, K_D is the generator damping coefficient, δ is the rotor angle (angle by which the quadrature axis leads the stator terminal voltage), and ω_0 is the reference speed ($2\pi f_0$).

The electrical torque T_e can be calculated as

$$T_e = P_e = P_t + R_a \cdot I^2$$

where P_e is the electrical active power, P_t represents the mechanical power, and R_a is the armature resistance per phase.

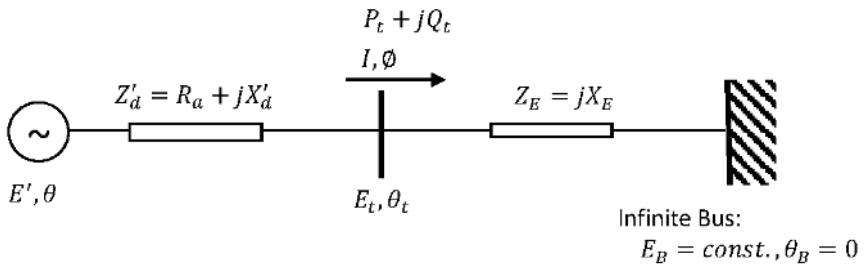

FIG. 1: Single machine infinite bus system.

3.1.2 Stator Electrical Equations

Electrical equations in the generator reference frame (lower case) are

$$e_d = -R_a \cdot i_d + X'_d \cdot i_q + e'_d$$

$$e_q = -R_a \cdot i_q + X'_d \cdot i_d + e'_q$$

where subscript "d" denotes the direct axis, "q" denotes the quadrature axis, and e and e' denote voltage and transient voltage in the generator reference frame. Voltages and currents are referred to a named generator reference frame that rotates at the generator's speed (direct axis "d" and quadrature axis "q"). Network and generator voltages and currents refer to a unique reference called the network reference frame that rotates at a constant synchronous speed. The relationship between machine internal voltage in the generator reference frame and in the network reference frame is listed as

$$E'_R = e'_d \cdot \sin\delta \ + e'_q \cdot \cos\delta$$

$$E'_I = e'_q \cdot \sin\delta \ - e'_d \cdot \cos\delta$$

where the subscripts R and I denote the network reference axes and E'_R, E'_I, and δ denote the "R" and "I" network components of transient voltages in the network reference frame and phase angle.

Stator equations in the network reference (upper case, subscripts R and I) are

$$\begin{bmatrix} E_R \\ E_I \end{bmatrix} = \begin{bmatrix} -R_a & X'_d \\ X'_d & -R_a \end{bmatrix} \begin{bmatrix} I_R \\ I_I \end{bmatrix} + \begin{bmatrix} E'_R \\ E'_I \end{bmatrix}$$

where E_R and E_I denote the "R" and "I" network components of voltages in the network reference frame.

The complex internal voltage and current are

$$\tilde{E}' = E'_R + j\ E'_I$$

$$\tilde{I} = \tilde{E}' \cdot \tilde{Y} = \frac{E'_R + j\ E'_I}{R_a + jX'_d}$$

where $\tilde{E}'$, $\tilde{I}$, and $\tilde{Y}$ are the complex transient internal voltage, current, and complex admittance matrix, respectively.

3.1.3 Network Representation and Static Loads

The general equation for a multibus network can be expressed in the following matrix form:

$$\tilde{\mathbf{I}} = \mathbf{Y_n} \cdot \tilde{\mathbf{V}}$$

where $\tilde{\mathbf{I}}$ and $\tilde{\mathbf{V}}$ are complex current injections and bus voltages in the network reference. $\mathbf{Y_n}$ is the admittance matrix that contains information on power line and static loads impedances and network connectivity.

For the case of a single machine infinite bus the previous equation is reduced to

$$\tilde{I} = \frac{1}{j\ X_E}\left(\tilde{E}_t - E_B\right)$$

where $\tilde{E}_t$, E_B, and X_E are the complex terminal voltage, infinite bus voltage, and transmission line reactance, respectively.

3.1.4 Initial Condition Calculation

The following equations can be used to initialize the generator model considering that the results of the power flow calculation (active power P_t, reactive power Q_t, and terminal voltage E_t) are used as the initial steady-state solution.

$$I = \frac{\sqrt{{P_t}^2 + {Q_t}^2}}{E_t}$$

$$\emptyset = \cos^{-1}\left(\frac{P_t}{E_t I}\right)$$

$$\delta = \tan^{-1}\left(\frac{X_d^{'} * I * \cos\emptyset \; - R_a * I * \sin\emptyset}{E_t + R_a * I * \cos\emptyset \; + X_d^{'} * I * \sin\emptyset}\right)$$

$$e_d = E_t \sin\delta$$

$$e_q = E_t \cos\delta$$

$$i_d = I \sin\left(\delta - \emptyset\right)$$

$$i_q = I \cos\left(\delta - \emptyset\right)$$

$$T_e = P_e = P_t + R_a I^2$$

3.1.5 Overall Equations

Differential and algebraic device equations, where devices are generators, dynamic loads, motors, etc., can be represented as

$$\dot{\mathbf{x}}_{\mathbf{d}v} = \mathbf{f}_{dv}\left(\mathbf{x}_{dv}, \mathbf{V}_{dv}\right)$$

$$\mathbf{I}_{dv} = \mathbf{g}_{dv}\left(\mathbf{x}_{dv}, \mathbf{V}_{dv}\right)$$

where $\mathbf{f}_{dv}$ and $\mathbf{g}_{dv}$ are the functions that describe the differential and algebraic device equations, $\mathbf{x}_{dv}$ is the state vector of the individual device, $\mathbf{I}_{dv}$ are the R and I network components of the current injection from the individual device into the network, and $\mathbf{V}_{dv}$ are the R and I network components of the bus voltages.

Grouping all the device differential equations and all the device algebraic equations with the network algebraic equations, the following general formulation is obtained:

$$\dot{\mathbf{x}} = \mathbf{f}\left(\mathbf{x}, \mathbf{V}\right)$$

$$\mathbf{I}\left(\mathbf{x}, \widetilde{\mathbf{V}}\right) = \mathbf{Y_n} \cdot \mathbf{V}$$

where $\mathbf{x}$ is the state vector of the system, $\mathbf{f}(\mathbf{x}, \mathbf{V})$ is the function describing the system differential equations, $\mathbf{I}$ is the current injection vector, $\mathbf{Y_n}$ is the node admittance matrix, and $\mathbf{V}$ is the bus voltage vector.

This system can be solved using numerical integration methods either simultaneously or partitioned. The simultaneous method is numerically more stable [power systems analysis toolbox (PSAT) uses this method]. For a description of the two basic solution schemes see [29], Section 13.3.6.

3.2 UQ for the Single Machine Infinite Bus System

To demonstrate the uncertainty quantification capability and illustrate the application of PCM on a sparse grid points approach, the single machine infinite bus system shown in Fig. 1 is used. The previous section provides the detailed formulation for the single machine infinite bus system. The uncertainty, which is described as $X'_d = \overline{X'_d}(1 + 10\%\zeta)$ and $M = \overline{M}(1 + 10\%\varepsilon)$, is assumed to come from the generator transient reactance (X'_d) and generator mass (H), due to lack of accurate knowledge and system variations over time. We assume such uncertainties have uniform distribution. Here, $\overline{X'_d}$ and $\overline{M}$ are the corresponding mean values of generator transient reactance (X'_d) and generator mass (M). ζ and ε are modeled by two uniform random variables [–1,1]. The standard deviation of generator transient reactance and generator mass are $0.1\overline{X'_d}\sigma_\zeta$ and $0.1\overline{M}\varepsilon$, respectively. There are two uncertain parameters total in the single machine infinite bus system model. Two different uncertainty quantification techniques are employed here: one is PCM on sparse grids, and the other is MC simulations. Large numbers of MC simulations are performed to verify the correctness of the PCM results.

Figure 2 shows the mean and standard deviation of omega speed as a function of time with different numbers of sparse grids, N_c = 5, 13, 29, and 65. Observe that the four curves of the mean of omega speed overlap each other,

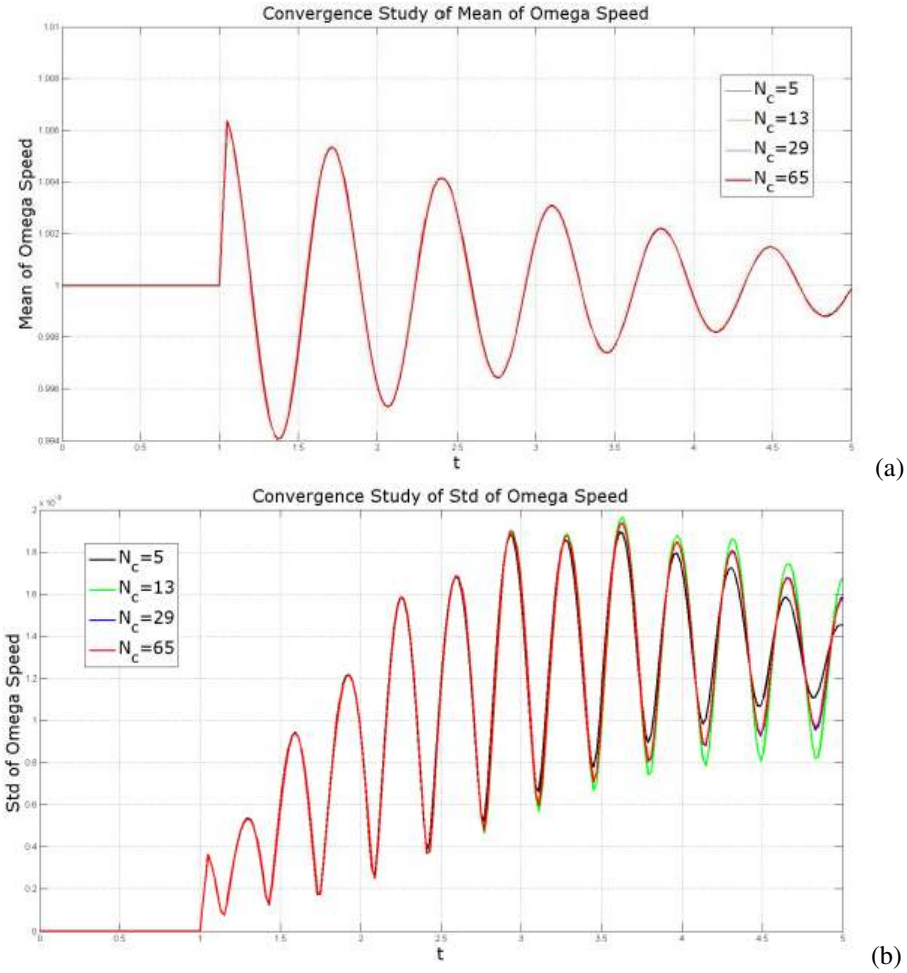

FIG. 2: (a) Mean and (b) standard deviation of omega speed as a function of time obtained by the probabilistic collocation method with different numbers of sparse grid points. The uncertainty comes from the generator transient reactance (X'_d) and generator mass (M).

while the four curves of the variance of omega speed agree well for $t < 3$, then the curves representing the results of N_c = 5 and 13 start to deviate from the results of N_c = 29 and 65. Figure 2 demonstrates the fast convergence for PCM. A larger number of sparse grid points are necessary to get an accurate standard deviation value than mean value. This is because high-order moments need more samplings to resolve.

Figures 3 and 4 present the mean and the standard deviation of delta angle and terminal voltage as a function of time with the number of sparse grids, N_c = 5, 13, 29, and 65, respectively. Good agreements are observed, which demonstrate fast convergence for PCM. The standard deviation results in Figs. 3 and 4 indicate that as time increases, we need more sparse grid points to obtain accurate standard deviation results.

Figure 5 shows the deterministic solution, mean, and error bar of omega speed and terminal voltage as a function of time using PCM. As time increases, the uncertainty effect also increases, which is probably due to the total uncertainty accumulated over time. Additionally, it is obvious that the deterministic value is different from the mean value for omega speeds.

Figure 6 presents the deterministic solution, mean, and error bar of delta angle as a function of time, and the eigenvalues of the linearized system. The error bar of the delta angle increases over time. The region on the left

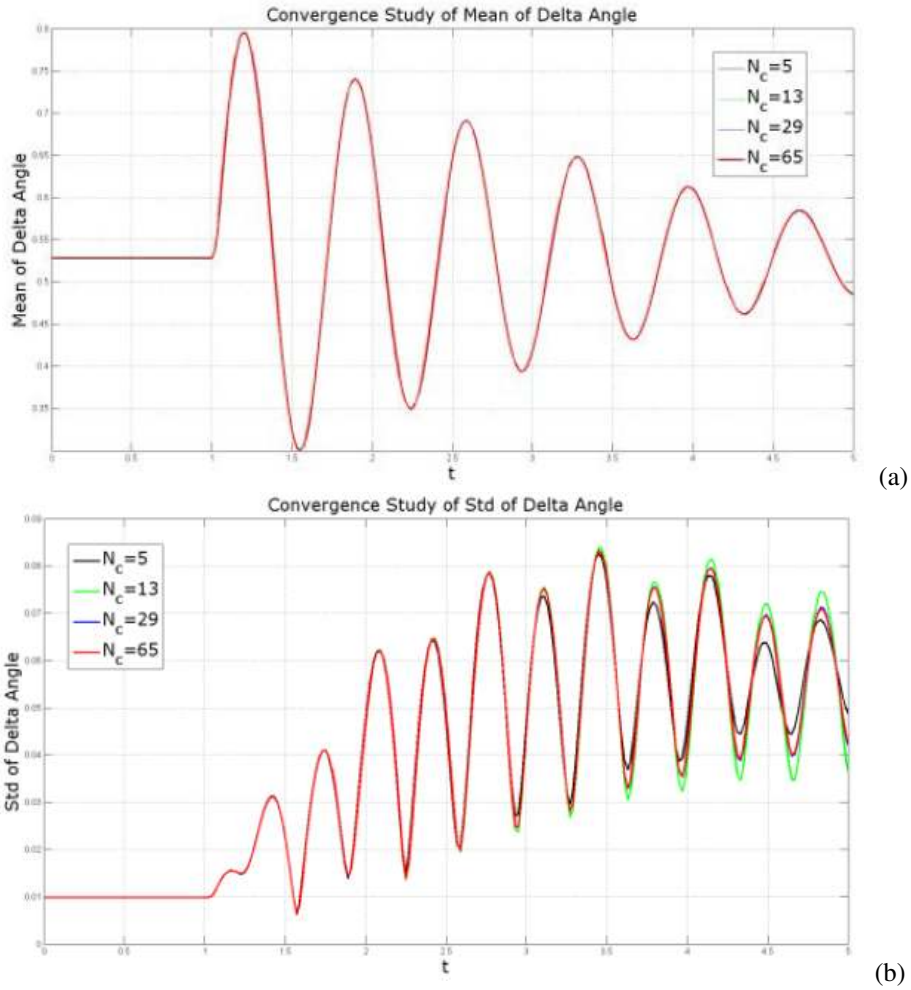

FIG. 3: (a) Mean and (b) standard deviation of delta angle as a function of time obtained by the probabilistic collocation method with different numbers of sparse grid points. The uncertainty comes from the generator transient reactance (X'_d) and generator mass (M).

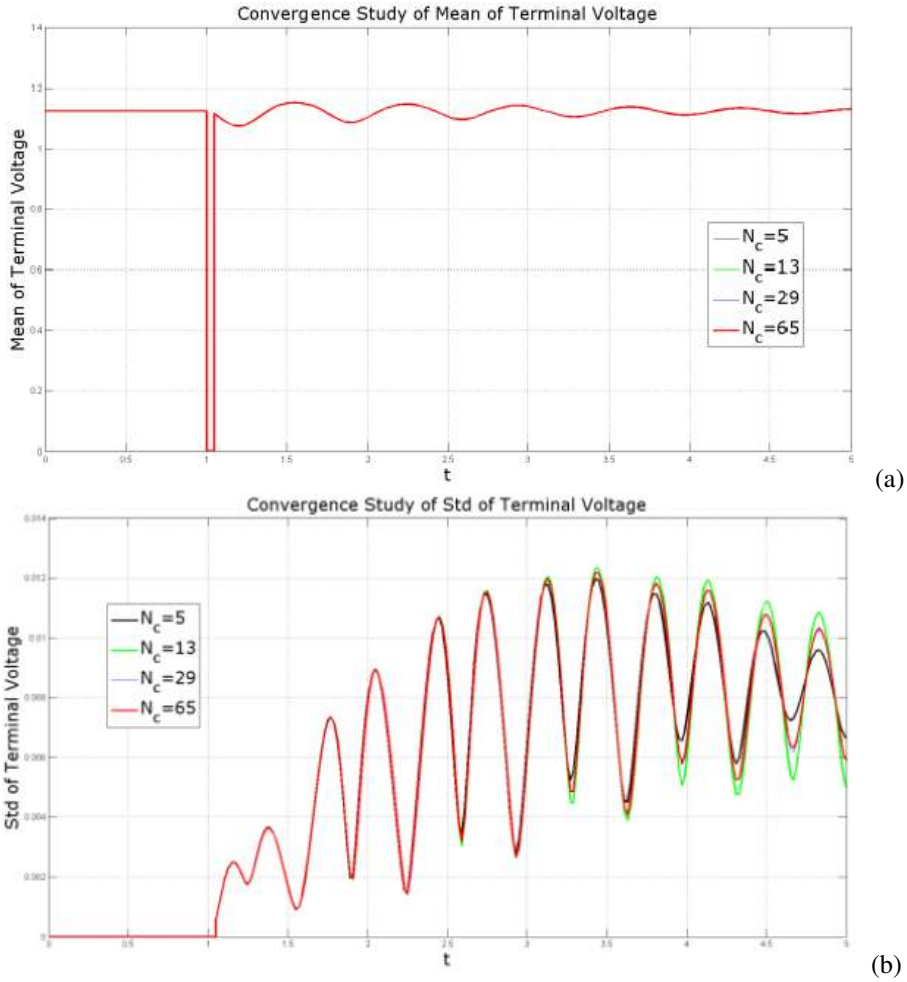

FIG. 4: (a) Mean and (b) standard deviation of terminal voltage as a function of time obtained by the probabilistic collocation method with different numbers of sparse grid points. The uncertainty comes from the generator transient reactance (X'_d) and generator mass (M).

side of the red lines in Fig. 6(b) indicates the acceptable stable region with enough damping, while the right side of the red lines indicates the unacceptable region which is still stable but without enough damping. Although both the deterministic and mean eigenvalues are located within the acceptable region, the error bar of the eigenvalue is across the acceptable region, which indicates that the uncertainty could cause the single machine infinite bus model to have large oscillations with unacceptable damping.

3.3 UQ for the WECC Power System Model

In the previous section, we have validated the PCM on the single machine infinite bus model. In the following discussion we will investigate the capability of the PCM on sparse grids on quantifying the uncertainty for a large-scale dynamic power system—the WECC power system model. The power system model and contingencies used in the uncertainty quantification analysis can be described as follows.

The dynamic model of power systems contain algebraic (nonlinear) and differential (first-order) equations, representing major elements in the systems, including generators, generator controllers such as governors and automatic

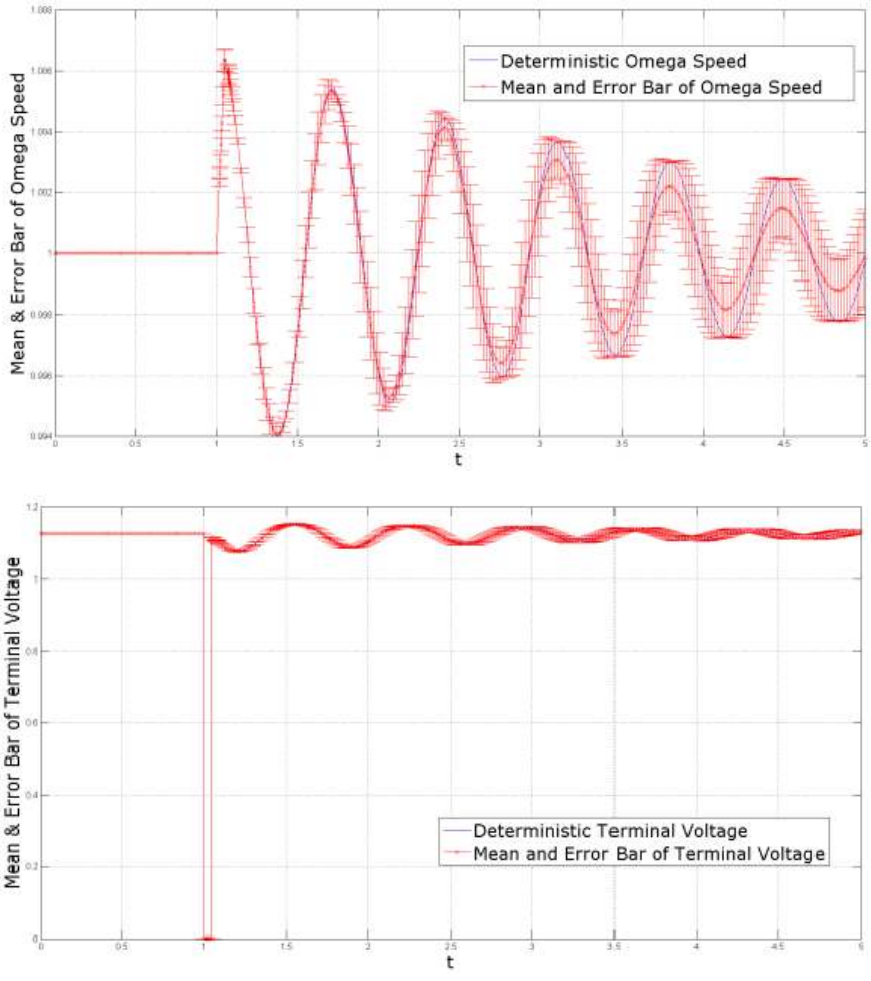

FIG. 5: Deterministic solution, mean, and error bar of (a) omega speed and (b) terminal voltage as a function of time. The uncertainty comes from the generator transient reactance (X'_d) and generator mass (M).

voltage regulators, transmission lines, and loads. Some elements of the protection system are also represented, such as undervoltage relays and overexcitation limiter relays. The full WECC model was used in this study.

Figure 7 shows a diagram of the WECC system model which is composed of approximately 14,324 power lines, 6533 transformers, 16,384 buses, 8230 load models, and 3307 generators. A base case representing the summer of 2010 was modified to represent a stressed precontingency condition. The modifications included: setting out of service two 500 kV lines and a 500/23 kV transformer near the California–Oregon intertie (COI). Additionally, the generation pattern was modified to increase the power transfer in the COI from 3970 to 4400 MW. These stressed conditions are similar to the precontingency conditions of the August 1996 systemwide outage. The load model used in the summer 2010 WECC model consisted of an 80% polynomial model and 20% motor load model, as it is was defined in [30]. In reality, the percentage and dynamic characteristics of the motor load change as operating condition and weather conditions change.

Two contingencies were simulated in the stressed power system model. The contingencies included a trip of two 500 kV power lines at a simulation time of 2 s, and two large generation units tripped in the south at a simulation time of 10 s. Figure 8 shows the evolution of the voltage at one of the buses of the COI; the contingencies and relay actions are indicated in the figure. The figure shows the results for 10%, 20%, and 30% of motor loads distributed across the

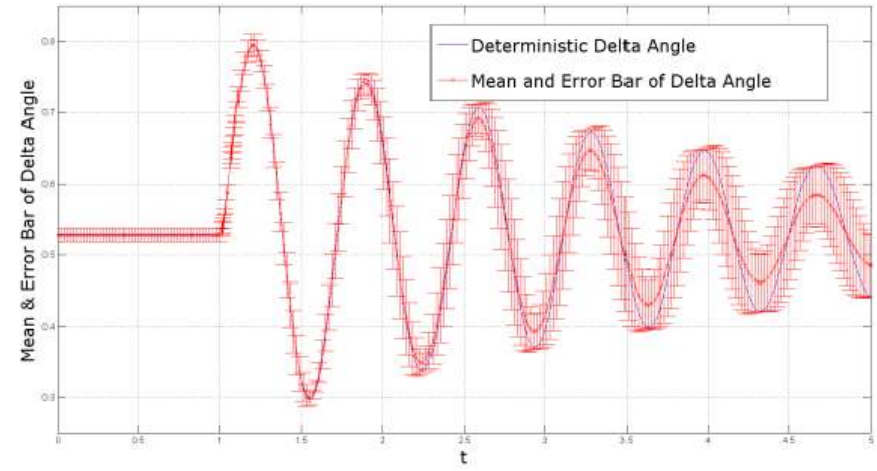

(a)

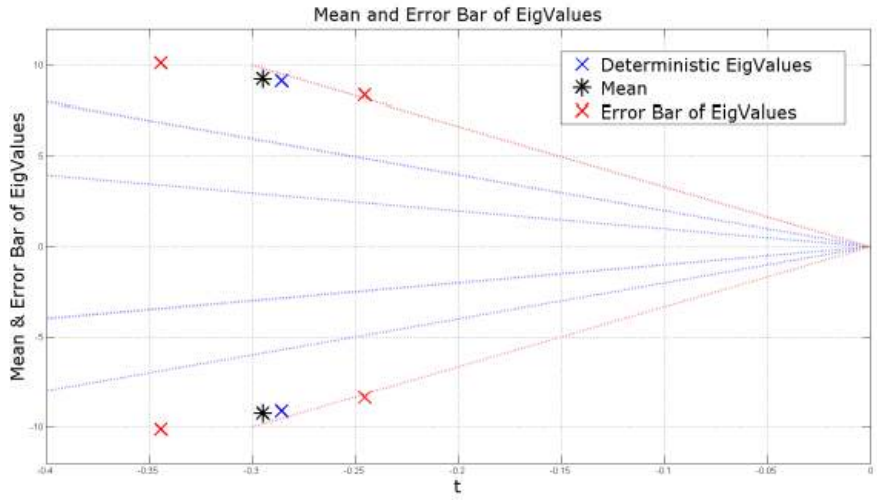

(b)

FIG. 6: Deterministic solution, mean, and error bar of (a) delta angle and (b) eigenvalue as a function of time. The uncertainty comes from the generator transient reactance (X'_d) and generator mass (M).

system. It can be seen that the system response changes for the different percentages of load represented by motor loads, particularly between 10 and 15 s and after 35 s of simulation.

Due to uncertainties with model parameters, we want to quantify the uncertainty of some important bus voltages, frequencies, and phase angles. Difficulty arises from the nonlinearity of the models, which makes the propagation of uncertainty difficult to analyze analytically. Numerical simulations are too time-consuming for large systems. For example, simulating 30 s of a WECC system model takes 3$\sim$4 min on a modern PC.

3.4 UQ for the WECC Power System Model–Two Uncertain Parameters Case

Here the uncertainty in the WECC model is assumed to be dominated by the uncertainty in motor load in the northern and southern part of the system, which is divided as shown in Fig. 7. In other words, only two parameters are assumed uncertain: the percentage of motor load in the north of the WECC, and the percentage of motor load in the south of the WECC. The north mean motor load is assumed to be 20% of the total load and the standard deviation of the north motor load is 10% of the total load. The south mean motor load is assumed to be 15% of the total load and the standard

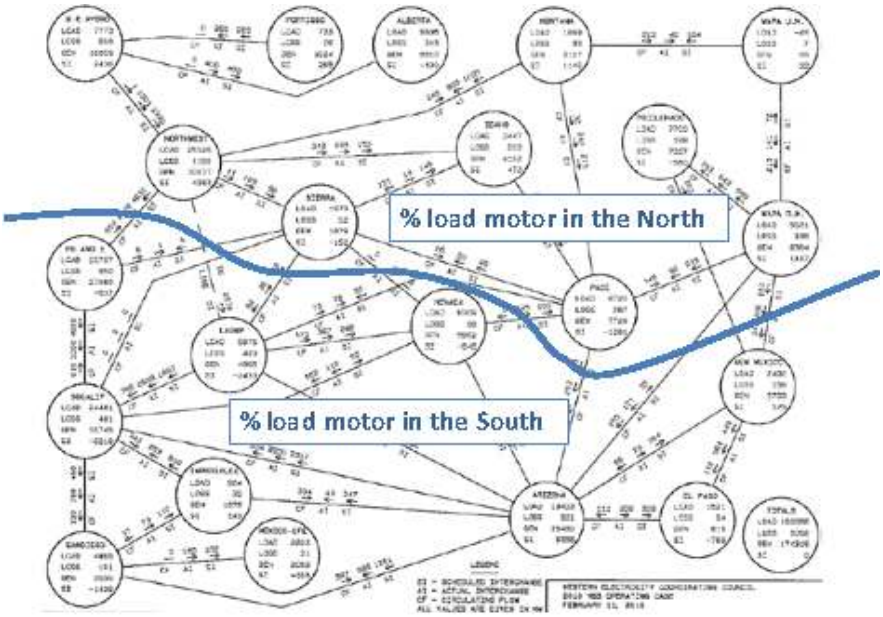

FIG. 7: Diagram of WECC interconnection power system model.

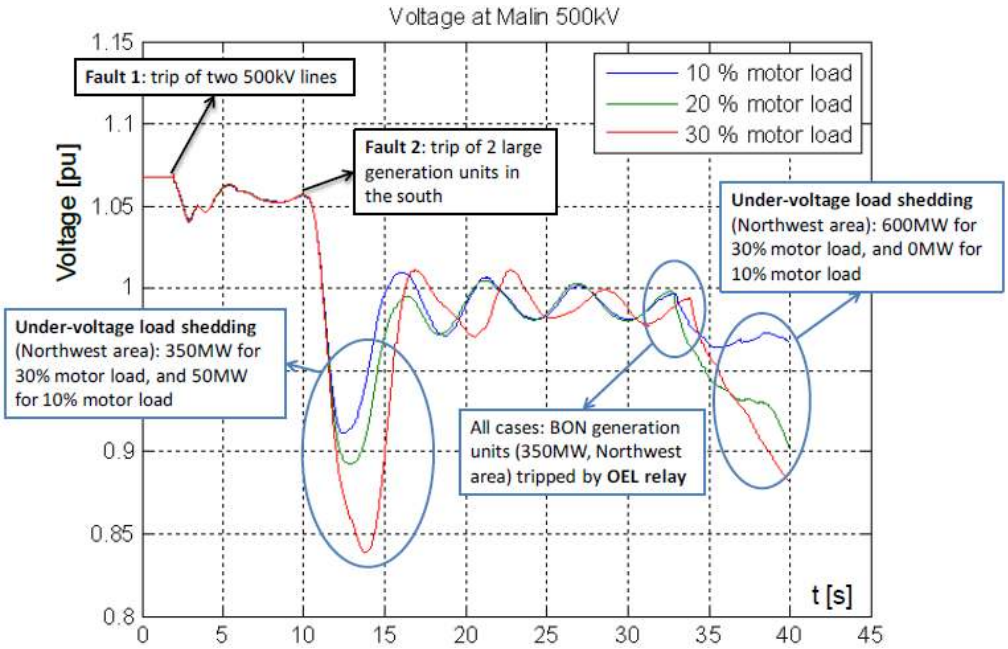

FIG. 8: Voltage at a bus in the COI.

deviation of the south motor load is 5% of the total load. Both north motor load and south motor load are modeled by uniform random variables.

In Fig. 9, we demonstrate the mean and error bar of the phase angle difference and active power flow on California Oregon Intertie (COI). using the PCM and MC methods. Good agreement is observed between the numerical results obtained from 1000 MC simulations and 65 stochastic collocation sparse grid points. It is obvious that using the

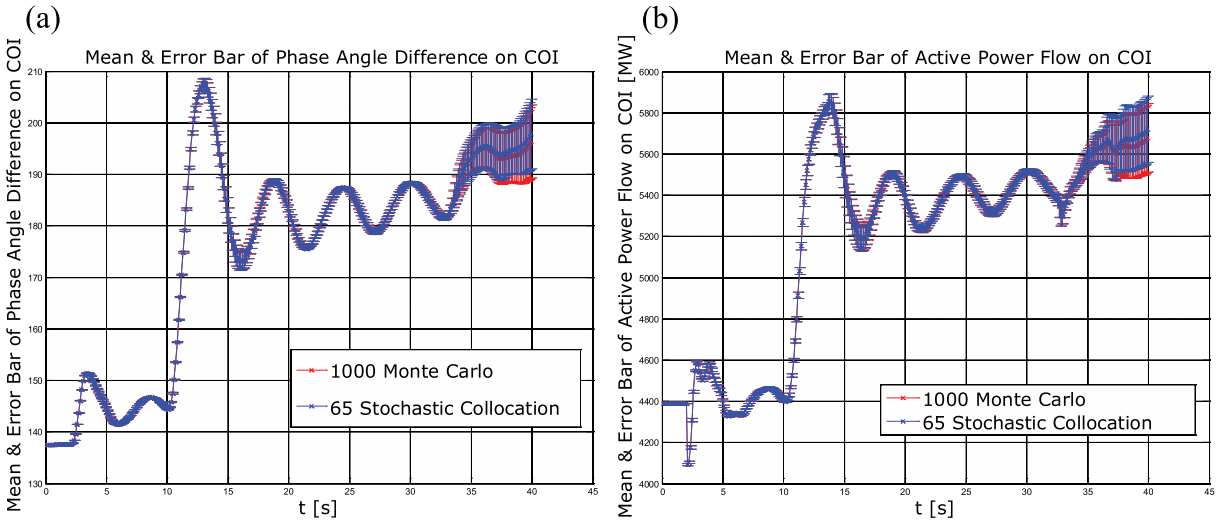

FIG. 9: Mean and error bar of (a) phase angle difference and (b) active power flow on COI using the probabilistic collocation method and MC method.

PCM can greatly reduce the computational cost and speed up the UQ process. A large error bar and some differences between the results from the MC simulation and the PCM results can be observed beyond $t = 35$ s, which is due to the power system instability. To quantify the uncertainty with a large variance (large error bar) beyond $t = 35$ s, more probabilistic collocation sparse grid points are necessary.

Figure 10 presents the mean and error bar of voltage at the Malin 500 KV turbine and active power flow on COI using PCM on 65 sparse grid points and 1000 MC simulations. Good consistency is observed between the results obtained by the PCM approach and ones by MC simulations. The results show that the MC method requires 1000 samples, while the collocation method only requires 65 samples to reach a similar level of estimation accuracy in quantifying the prediction uncertainty. Hence, it is evident that the PCM approach could greatly reduce the computational cost and speed up the UQ process.

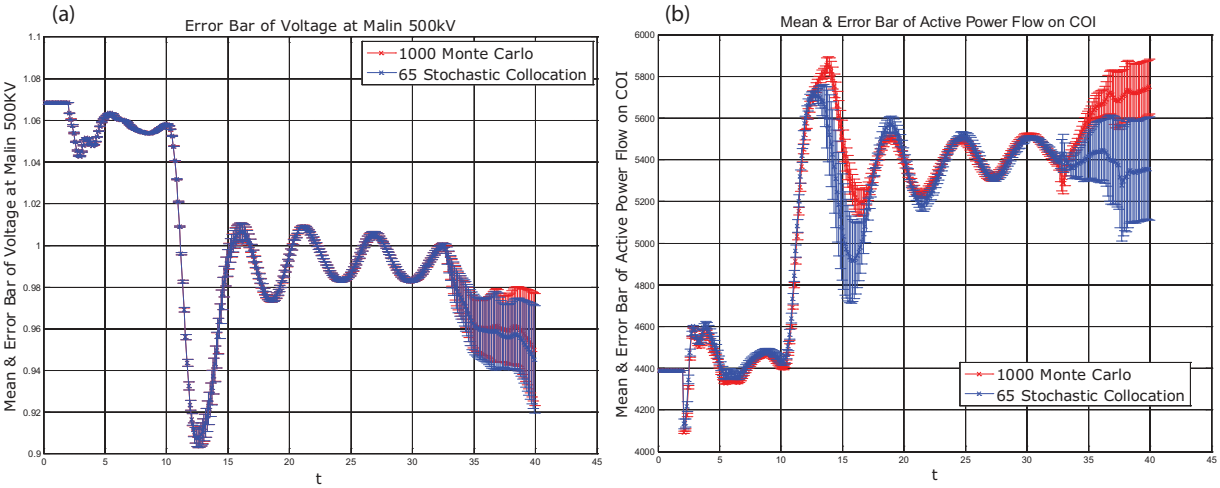

FIG. 10: Mean and error bar of (a) voltage at Malin 500 KV and (b) active power flow on COI using PCM on 65 sparse grid points and 1000 MC simulations.

3.5 for the WECC Power System Model–21 Uncertain Parameters Case

In this case the uncertainty in the WECC model is assumed to be dominated by the uncertainty in the percentage of motor load for each of the following 21 areas that compose the WECC system (New Mexico, El Paso, Arizona, Nevada, Mexico-CFE, ImperialCA, San Diego, Socalif, LADWP, PG&E, Northwest, B.C.Hydro, FORTISBC, Alberta, Idaho, Montana, WAPA U.M., Sierra, PACE, PSColorado, and WAPA R.M.). The standard deviation of the percentage of motor load in each area is assumed to be 10% of the mean percentage of motor load. The percentage of motor load is modeled by uniform random variables.

Figure 11 presents the mean and error bar of voltage at Malin 500 KV and Palo Verde 500 KV using PCM on 43 sparse grid points and 1000 MC simulations. The results obtained by the PCM approach matches with the results from 1000 MC simulations. Figure 11 also indicates that more collocation points are needed to match the error bar (variance) results than the mean results, especially for times beyond 35 s, where instability happens. Figure 12 plots the mean and error bar of voltage at GM Shrum 500 KV and frequency at Malin 500 KV using PCM on 43 sparse grid

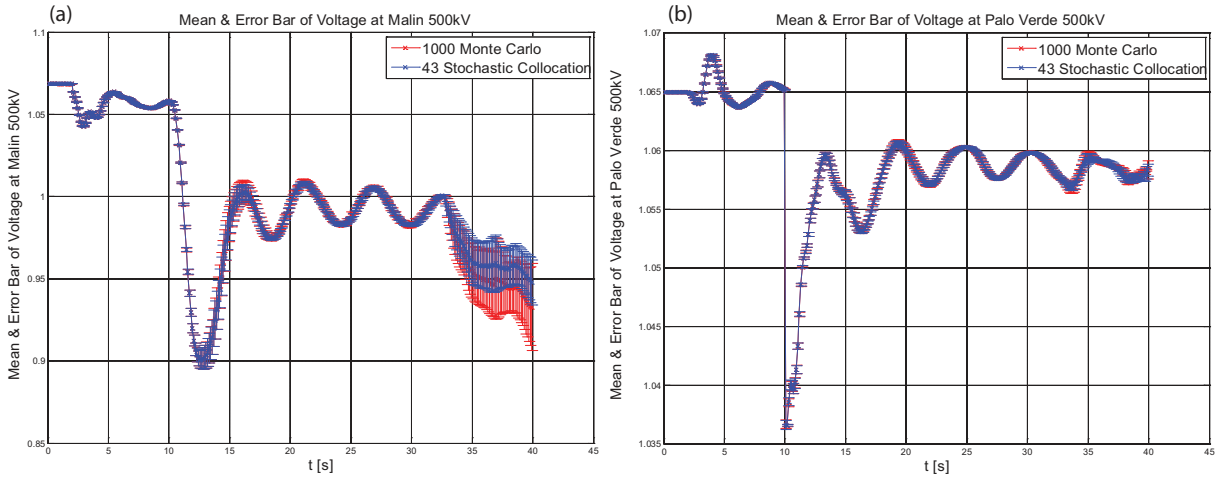

FIG. 11: Mean and error bar of voltage at (a) Malin 500 KV and (b) Palo Verde 500 KV using PCM on 43 sparse grid points and 1000 MC simulations.

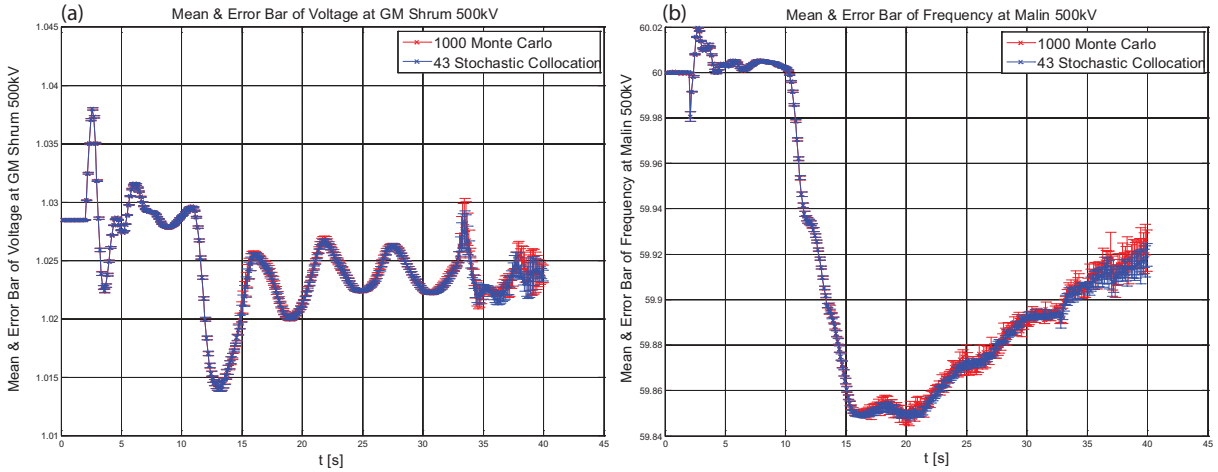

FIG. 12: Mean and error bar of (a) voltage at GM Shrum 500 KV and (b) frequency at Malin 500 KV using PCM on 43 sparse grid points and 1000 MC simulations.

points and 1000 MC simulations. Similarly, the results obtained by the PCM approach are in good agreement with the results from 1000 MC simulations.

Figure 13 presents the mean and error bar of frequency at Palo Verde 500 KV and GM Shrum 500 KV using PCM on 43 sparse grid points and 1000 MC simulations. In Fig. 14, we show the mean and error bar of COI power transfer using PCM on 43 sparse grid points and 1000 MC simulations. Good agreement is observed in both Figs. 13 and 14 between the results obtained by the PCM approach and the results from 1000 MC simulations.

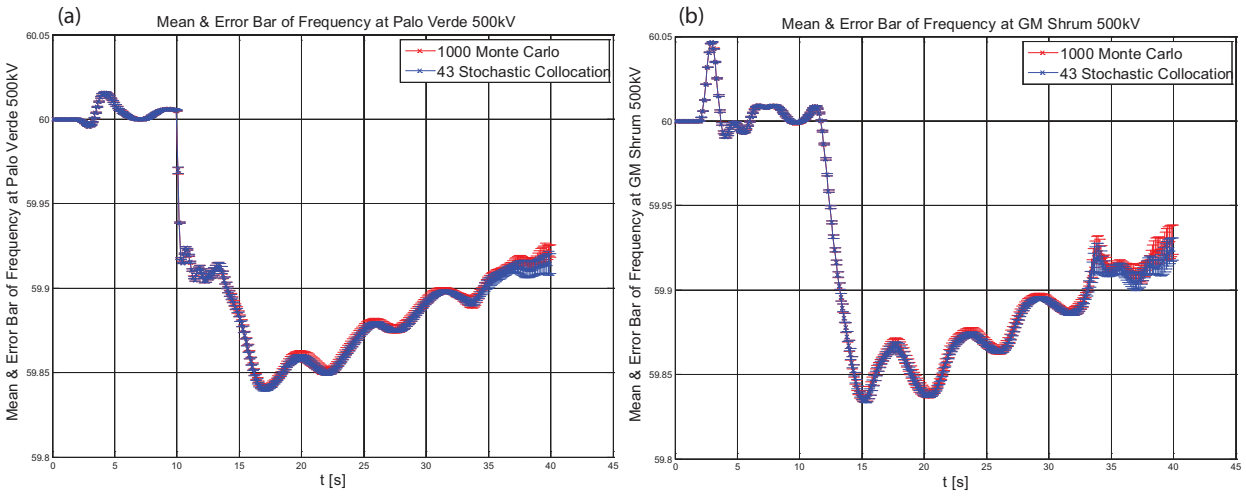

FIG. 13: Mean and error bar of frequency at (a) Palo Verde 500 KV and (b) GM Shrum 500 KV using PCM on 43 sparse grid points and 1000 MC simulations.

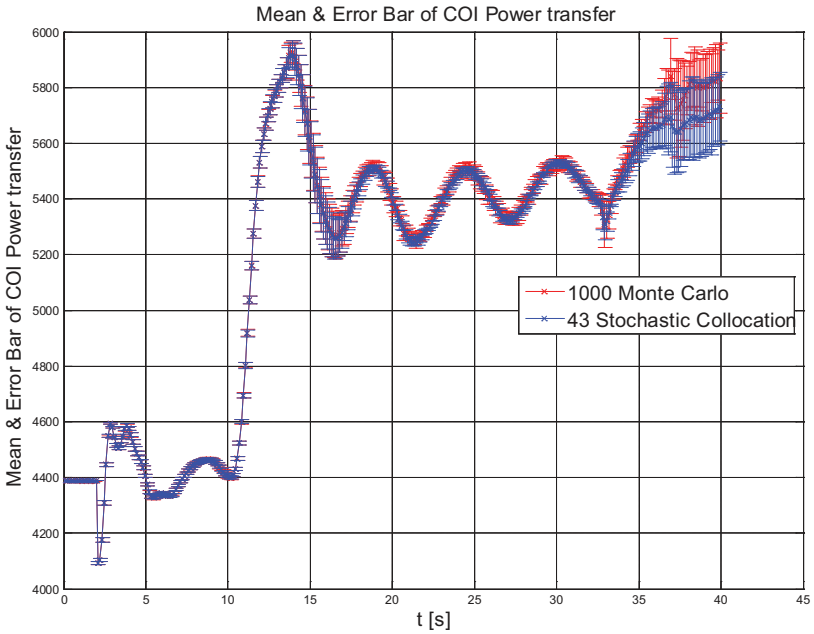

FIG. 14: Mean and error bar of COI power transfer using PCM on 43 sparse grid points and 1000 MC simulations.

4. CONCLUSION

A new, efficient UQ technique, the PCM approach on sparse grids, is introduced to evaluate the uncertainty in a single machine infinite bus system and the large-scale WECC system in western North America. The PCM is able to efficiently quantify the uncertainty in nonlinear complex dynamic systems, such as the WECC system, and allow the use of just a small number of sparse grid points to quantify the uncertainty in power system dynamic modeling. By using the sparse grid points, the PCM approach can quantify the uncertain parameters in power systems with relatively lower computational cost when compared with classic MC simulations. This paper demonstrated the capability and illustrated the application of PCM on sparse grid points approach on UQ using the single machine infinite bus system and the large-scale WECC system as an example. MC simulations have also been conducted to verify accuracy of the PCM approach. By comparing the results obtained from MC simulations with PCM results for the mean and standard deviation of uncertain parameters, it is evident that the PCM approach is computationally more efficient than MC simulations. Our future work will focus on employing the adaptive hierarchical sparse grid PCM [31, 32] and adaptive high-dimensional stochastic model representation technique [33–35] to quantify large-number uncertainty parameters in dynamic simulations of large-scale power system models.

ACKNOWLEDGMENT

This work was supported by the Applied Mathematics program of the DOE Office of Advanced Scientific Computing Research. A portion of the computations was performed using PNNL Institutional Computing cluster systems, as well as computational resources from the National Energy Research Scientific Computing Center at Lawrence Berkeley National Laboratory. PNNL is operated by Battelle for the DOE under Contract DE-AC05-76RL01830. The authors thank the anonymous reviewers for their valuable comments and suggestions.

REFERENCES

1. Ali, A., and Gomez-Exposito, A., *Power System State Estimation*, Taylor & Francis, London, 2004.
2. Monticelli, A., Electric power system state estimation, *Proc. IEEE*, 88:262–282, 2000.
3. Monticelli, A., *State Estimation in Electric Power Systems—A Generalized Approach*, Kluwer, Norwell, MA, 1999.
4. Gautam D., Vittal, D., and Harbour, T., Impact of increased penetration of DFIG-based wind turbine generators on transient and small signal stability of power systems, *IEEE Trans. Power Syst*., 24:1426–1434, 2009.
5. Kosterev, D. N., Meklin, A., Undrill, J., Lesieutre, B., Price, W., Chassin, D., Bravo, R., and Yang, S., Load modeling in power system studies: WECC progress update, *IEEE Power and Energy Society General Meeting*, pp. 1–8, Pittsburgh, PA, 20–24 July, 2008.
6. Pereira L., Undrill J., Kosterev, D., Davies, D., and Patterson S., A new thermal governor modeling approach in the WECC, *IEEE Trans. Power Syst*., 18(2):819–829, 2003.
7. Kosterev, D. N., Taylor, C. W., and Mittelstadt, W. A., Model validation for the August 10, 1996 WSCC system outage, *IEEE Trans. Power Syst*., 14(3):967–979, 1999.
8. Western Electricity Coordination Council, http://www.wecc.biz, 2012.
9. Julier, S. J., The scaled unscented transformation, *Proc. Am. Control Conf*., 6:4555–4559, 2002.
10. Hiskens, I. A., Pai, M. A., and Nguyen, T. B., Bounding uncertainty in power system dynamic simulations, in *IEEE Power Engineering Society Winter Meeting*, Singapore, 23–27 Jan., 2000.
11. Hockenberry, J. R. and Lesieutre, B. C., Evaluation of uncertainty in dynamic simulations of power system models: The probabilistic collocation method, *IEEE Trans. Power Syst*., 19(3):1483–1491, 2004.
12. Kyriakides, E., and Heydt, G. T., Calculating confidence intervals in parameter estimation: A case study, *IEEE Trans. Power Delivery*, 21(1):508–509, 2006.
13. Al-Othman, A. K., A fuzzy state estimator based on uncertain measurements, *J. Int. Measure. Confed*., 42(4):628–637, 2009.
14. Al-Othman, A. K. and Irving, M. R., Uncertainty modeling in power system state estimation, *IEE Proc.: Gener. Transm. Distrib.*, 152:233–239, 2005.

15. Al-Othman, A. K. and Irving, M. R., Analysis of confidence bounds in power system state estimation with uncertainty in both measurements and parameters, *Electr. Power Syst. Res*., 76(12):1011–1018, 2006.
16. Lucor, D., Su, C.-H., and Karniadakis, G. E., Generalized polynomial chaos and random oscillators, *Int. J. Numer. Methods Eng*., 60(3):571–596, 2004.
17. Tatang, M. and McRae, G., Direct treatment of uncertainty in models of reaction and transport, Technical Report, MIT Technical Report, 1994.
18. Xiu, D. and Hesthaven, J. S., High order collocation methods for differential equations with random inputs, *SIAM J. Sci. Comput*., 27(3):1118–1139, 2005.
19. Ghanem, R. G. and Spanos, P., *Stochastic Finite Elements: A Spectral Approach*, Springer-Verlag, New York, 1991.
20. Cools, R., Monomial cubature rules since "Stroud": A compilation, *J. Comput. Appl. Math*., 48:309–326, 1993.
21. Cools, R., Monomial cubature rules since "Stroud": A compilatio—Part 2, *J. Comput. Appl. Math*., 112:21–27, 1999.
22. Su, Q. and Strunz, K., Stochastic polynomial-chaos-based average modeling for power electronic systems, *IEEE Trans. Power Electron*., 26(4):1167–1171, 2011.
23. Strunz, K. and Su, Q., Stochastic formulation of SPICE-type electronic circuit simulation with polynomial chaos, *ACM Trans. Model. Comput. Simul*., 18(4):15:1–15:23, 2008.
24. Su, Q. and Strunz, K., Circuit branch modelling for stochastic analysis with Hermite polynomial chaos, *Electron. Lett*., 41(21):1163–1165, 2005.
25. Su, Q. and Strunz, K., Stochastic polynomial-chaos-based average model of twelve pulse diode rectifier for aircraft applications, in *IEEE Workshops on Computers in Power Electronics*, Troy, NY, July, 2006.
26. IEEE power system 14 bus test case, Electric Engineering, University of Washington, http://www.ee.washington.edu/research/pstca/, 2012.
27. Julier, S. and Uhlmann, J. K., A general method for approximating nonlinear transformations of probability distributions, Technical Report, Robotics Research Group, Department of Engineering Science, University of Oxford, 1996.
28. Julier, S. J. and Uhlmann, J. K., A new extension of the Kalman filter to nonlinear systems, in *Proc. of AeroSense: The 11th Intl. Symp. on Aerospace/Defense Sensing, Simulation and Controls*, Orlando, FL, 1997.
29. Kundur, P., *Power Systems Stability and Control*, McGraw-Hill, Inc., New York, 1994.
30. Pereira L., Kosterev, D., Mackin, P., Davies, D., Undrill J., and Zhu, W., An interim dynamic induction motor model stability studies in the WSCC, *IEEE Trans. Power Syst*., 17:1108–1115, 2002.
31. Ma, X. and Zabaras, N., An adaptive hierarchical sparse grid collocation algorithm for the solution of stochastic differential equations*, J. Comput. Phys*., 228:3084–3113, 2009.
32. Ganapathysubramanian B. and Zabaras, N., Sparse grid collocation methods for stochastic natural convection problems, *J. Comput. Phys*., 225:652–685, 2007.
33. Ma, X. and Zabaras, N., An adaptive high-dimensional stochastic model representation technique for the solution of stochastic PDEs, *J. Comput. Phys*., 229(10):3884–3915, 2010.
34. Yang, X., Choi, M., Lin, G., and Karniadakis, G. E., Adaptive ANOVA decomposition of incompressible and compressible flows, *J. Comput. Phys*., 231(4):1587–1614, 2012.
35. Lin, G., Tartakovsky, A. M., and Tartakovsky, D. M., Uncertainty quantification via random domain decomposition and probabilistic collocation on sparse grids, *J. Comput. Phys*., 229(19):6995–7012, 2010.
36. Smolyak, S., Quadrature and interpolation formulas for tensor products of certain classes of functions, *Sov. Math. Dokl*., 4:240–243, 1963.
37. Morokoff W. J. and Caflisch, R. E., Quasi-Monte Carlo integration, *J. Comput. Phys*., 122(2):218–230, 1995.
38. Griebel, M., Adaptive sparse grid multilevel methods for elliptic pdes based on finite differences, *Computing*, 61(2):151–180, 1998.

APPENDIX A. CHOICES OF COLLOCATION POINTS

Without loss of generality, assume that the random vector variables ξ_k, $k = 1, ..., N_M$ are defined in $[-\infty, +\infty]^M$ with possible compact support, or that they have bounded support and can be represented by or mapped (when

possible) to an M hypercube, where M is the number of random dimensions (components) of the vector $\xi_k = \{\xi_{1,k}, \xi_{2,k}, ..., \xi_{M,k}\}^T$. For the prescribed number of collocation points, N_c, the computational cost of the PCM approach is N_c times the cost of the corresponding deterministic problem. Thus, for a given required accuracy, the goal is to choose the collocation point set with the minimal number of collocation points. The following sections describe two different methods for the selection of collocation point sets: (1) tensor products of one-dimensional collocation point sets and (2) sparse grids strategy for high dimensionality.

APPENDIX A.1 Tensor Products of One-Dimensional Collocation Point Sets

Due to its simplicity, the tensor product of a one-dimensional point set provides a straightforward choice of a collocation point set. For each random dimension $i = 1, ..., M$, a good one-dimensional interpolation formula can be constructed for a smooth function

$$\mathcal{U}^i(f) = \sum_{k=1}^{n_i} f(X_k^i) a_k^i \tag{A.1}$$

based on collocation point sets $\Theta^i = (X_1^i, ..., X_{n_i}^i)$, where $\mathcal{U}^i(f)$ is a one-dimensional interpolation formula to approximate the smooth function f, X_k^i is the collocation point k in the random dimension i, $a_k^i \equiv a_k(X^i)$ is the weight, and n_i is the number of collocation points in dimension i. A sequence of tensor products can be obtained for each random dimension i.

In the multivariate case ($M > 1$), the tensor product formula is

$$\mathcal{I}(f) = (\mathcal{U}_1^{i_1} \otimes ... \otimes \mathcal{U}_M^{i_M})(f) = \sum_{k_1=1}^{n_{i_1}} ... \sum_{k_M=1}^{n_{i_M}} f(X_{k_1}^{i_1}, ..., X_{k_M}^{i_M}) \cdot (a_{k_1}^{i_1} \otimes ... \otimes a_{k_M}^{i_M}). \tag{A.2}$$

Equation (A.2) needs N_c collocation points, where $N_c = N_{c_1} \cdots N_{c_M}$ and N_{c_i} is the number of collocation points in dimension i, $i \in [1, M]$. For a small number of random dimensions, M (e.g., $M \leq 3$), the tensor product of one-dimensional collocation point sets is a good choice for collocation point sets. However, N_c grows exponentially as the number of random dimensions of M increases. Thus, the tensor product of one-dimensional collocation point sets becomes less efficient in the case of M with its high number of random dimensions.

APPENDIX A.2 High Dimensionality and Sparse Grids

Due to its high degree of accuracy, the Gauss quadrature can be efficient for one-dimensional integration. However, the number of random dimensions increases very fast as the correlation length decreases, and if the number of random dimensions is not adequate, erroneous oscillations appear for both the mean and the variance. In multi dimensions, using grid sets based on the tensor products of one-dimensional constructs leads to a prohibitively large number of collocation points. To counteract this, the Smolyak algorithm [36] is used, which is a linear combination of a tensor product formula. The resulting grid set has a significantly smaller number of grids, when comparing the sparse grids with the full tensor product rule. Recently, [18] constructed a PCM extension based on sparse grids using the Smolyak algorithm [36]. Sparse grids do not depend as strongly on the dimensionality of the random space, and hence, it is more suitable for applications with large dimensional random inputs.

Consider an interpolation formula $\mathcal{I}(f)$ to approximate function $f(x)$ in the M-dimensional domain $\Gamma = \Gamma_1 \times \Gamma_2 ... \Gamma_M$, where Γ_i can be unbounded.

Smolyak's algorithm is given by the linear combination of the tensor product formula in such a way that an interpolation property for $M = 1$ is preserved for the $M > 1$ case. The Smolyak algorithm is given by

$$\mathcal{I}(f) \equiv A(q, M) = \sum_{q-M+1 \leq |i| \leq q} (-1)^{q-|i|} \cdot \begin{pmatrix} M-1 \\ q-|i| \end{pmatrix} \cdot (\mathcal{U}_1^{i_1} \otimes \cdot \otimes \mathcal{U}_M^{i_M}), \tag{A.3}$$

where $\mathcal{U}_j^{i_j}$ is the one-dimensional interpolation formula for each $\mathcal{U}_j^{i_j}$, $\mathcal{I}(f)$ is the Smolyak interpolation formula, and the sparseness parameter $q \geq M$ determines the order of the algorithm, $i = (i_1, ..., i_M)$ and $|i| = i_1 + i_2 + \cdots + i_M$.

Here, $i_j (j \in [1, M])$ represents the number of collocation points in a random dimension j. Set $k = q - M$ as the "level" of the Smolyak construction. To compute $A(q, M)$, the only requirement is to evaluate the function on the "sparse grid"

$$\Theta_M \equiv \cup_{q-M+1 \le |i| \le q} (\Theta_1^{i_1} \times ... \times \Theta_1^{i_M}), \tag{A.4}$$

where $\Theta_1^{i_j}$ represents a one-dimensional collocation point set at a random dimension j and Θ_M is denoted as the M-dimension collocation point set.

In the present work, sparse collocation point sets are generated by Gaussian quadrature points using a Gaussian formula. By choosing $2^{i-1} + 1$ number of Gaussian quadrature points, a 2^i degree of exactness can be achieved. Table 1 compares the number of sparse grid points produced by the Smolyak algorithm and the tensor products of one-dimensional collocation point sets with different M, but with comparable accuracy for each row. In Table 1, N_c is the number of Smolyak Gauss sparse grid points, $Z_M^k = (k+1)^M$ is the number of collocation points for the full set of tensor products, $k + 1$ is the number of collocation points in each random dimension, and M is the number of random dimensions.

It can be seen that as the number of random dimensions M increases, the number of Smolyak sparse grid points N_c becomes significantly less than Z_M^k. Table 1 shows that for a random dimension $M \le 3$, the number of Gauss sparse grid points N_c is larger than the full tensor polynomial space because duplicated collocation points with different weights are selected in sparse grids, which indicates that it is more efficient to utilize the full tensor polynomial space for the $M \le 3$ case. For $M = 32$, N_c is significantly less than Z_M^k. In practice, it is more efficient to use the sparse grids strategy such that $4 \le M \le 50$. For $M > 50$, because the rapidly growing number of sparse grid points due to high random dimensionality effectively reduces its efficiency, the MC and quasi-Monte Carlo approach [37] are preferred when compared against the sparse grids approach. Figure 15 shows the locations of the sparse grid points

TABLE 1: The degrees of freedom of the Gaussian sparse grid points, N_c, and the tensor polynomial space, Z_M^k.

M	q	K	N_c	Z_M^k
3	4	1	10	8
	5	2	52	27
	6	3	195	64
10	11	1	31	1024
	12	2	486	59,049
	13	3	5166	1,048,576

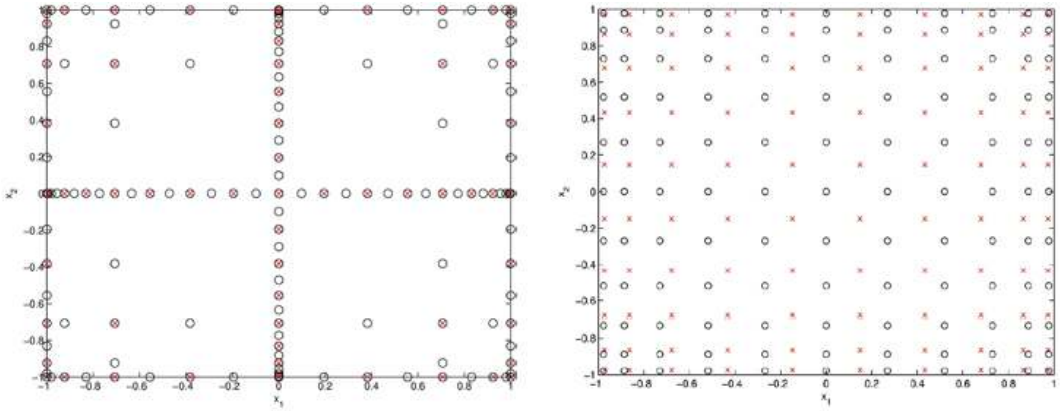

FIG. 15: Two random-dimensional $(M = 2)$ sparse grid points vs. full tensor products: (left) sparse grid level $k = 5$, $q = 7$ (cross nodes) and $k = 6$, $q = 8$ (circle nodes); (right) the corresponding full tensor products.

for $k = 5$ and 6, and the collocation points found from the full tensor products. Convergence is achieved if the numerical error in the random space between two successive spare grid levels is smaller than a specified threshold. Interested readers are referred to [38] for extensive reviews on the adaptivity of sparse grids.